

A28

Combined Seismic Waveform Inversion for Source Functions, Medium Parameters and Receiver Coupling Factors

H.R. Maurer* (ETH Zurich), S.A. Greenhalgh (ETH Zurich), S. Marelli (ETH Zurich), E. Manukyan (ETH Zurich) & A.G. Green (ETH Zurich)

SUMMARY

The quality of receiver-to-ground coupling can be highly variable in surface, surface-to-borehole, and crosshole seismic experiments. Poor coupling can affect the recorded seismic traces in a major way, such that ignoring variable coupling conditions can lead to severe problems when waveform inversions are attempted. To address this issue, we have developed a novel scheme that estimates medium properties and frequency-dependent source functions and frequency-dependent receiver-coupling factors. We demonstrate the efficacy of the new scheme via a synthetic crosshole experiment in which realistic receiver-coupling factors are simulated. Our simulations indicate that a combined inversion for source functions, medium parameters and receiver coupling factors yields results that are comparable to those obtained by using known receiver coupling factors (of course, this is only possible for simulations) and inverting for the source functions and medium parameters.

Introduction

Seismic tomography is a powerful and versatile tool for a wide range of imaging applications in the earth sciences. Crosshole techniques are of particular interest for shallow and intermediate target depths. Waveform inversion techniques are becoming increasingly popular (e.g., Plessix 2008, Buske et al. 2009), with frequency-domain algorithms proving to be particularly efficient (e.g., Pratt 1999, Zhou and Greenhalgh 2003).

The need to invert not only for the medium parameters, but also for the generally unknown source function is well known (e.g., Pratt 1999, Ernst et al. 2007). However, it is usually assumed that the response of the receivers can be ignored. This assumption may appear to be reasonable, because seismic receivers are typically selected to provide a flat response in the frequency band of interest, but the receiver-to-ground coupling may influence the recordings significantly. More seriously, the coupling behavior may vary from sensor to sensor. This problem is highlighted in the two source gathers of Figure 1. The seismic traces in this figure were acquired in the framework of a time-lapse crosshole experiment designed for the non-intrusive monitoring of buried radioactive waste (Manukyan et al. 2008). Seismic energy was generated by a high-frequency sparker placed in a $\sim 20^\circ$ downward-inclined borehole and the energy was received by a string of 24 hydrophones placed in a $\sim 20^\circ$ upward-inclined borehole. Both boreholes were water filled. More details on this experiment can be found in Marelli et al. (2010). During the acquisition of the first suite of data (example traces are shown in blue in Figure 1), the location of the hydrophone string was fixed and the sparker was sequentially ignited at 24 positions along the source borehole. Immediately afterwards, the hydrophone string was removed and reinserted at the same position in the receiver borehole (to within < 3 cm). The second suite of measurements (example traces are shown in red in Figure 1) were made by igniting the sparker at the same source positions (to within < 3 cm). The elastic parameters within the area of interest did not change between the two experiments, and extensive tests demonstrated that the repeatability of the seismic source was very good (Marelli et al. 2010). Consequently, variable receiver coupling must have produced the very significant differences between the blue and red traces. The astonishingly large differences are likely caused by minor changes in the seating of the hydrophones on the borehole wall; note, that we have also observed similar (although smaller) effects in data received by hydrophones hanging freely in vertically oriented boreholes. As a result of our experiments, we consider that it is necessary to have a waveform inversion algorithm that is capable of simultaneously estimating medium properties and frequency-dependent source functions and frequency-dependent receiver-coupling factors.

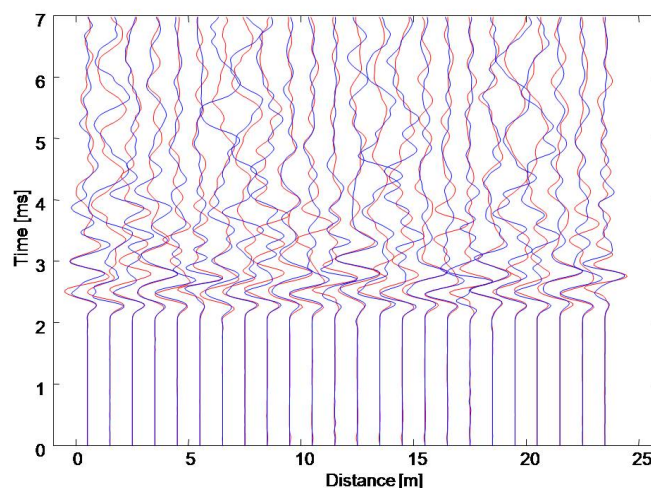


Figure 1: Results from a reinsertion experiment using a sparker source and a hydrophone string. The blue traces show a source gather from the first experiment and the red traces show the repeat source gather after reinserting the hydrophone streamer. Distance of the source from the borehole mouth is shown on the horizontal axis. Average source-receiver distances are 10-15 m. Note, that the first breaks were horizontally aligned for display purposes.

Methodology

For the sake of simplicity, we consider a 2D acoustic and constant-density problem that will be analyzed in the frequency domain. The observed and predicted data $d^{obs,pred}$ can be written as the product

$$(1) \quad d_{ij}(\omega) = s_i(\omega) \cdot G_{ij}(\mathbf{m}, \omega) \cdot r_j(\omega),$$

where i and j are the source and receiver indices, ω is frequency, s_i and r_j represent the unknown source functions and receiver-coupling factors, respectively, G_{ij} are the Green's functions that characterise wave propagation between the i th source and the j th receiver and the vector \mathbf{m} contains the medium properties (i.e. P-wave velocities).

To invert for the medium properties alone, an iterative Gauss-Newton type algorithm can be employed (e.g., Pratt et al. 1998)

$$(2) \quad \mathbf{m}_{k+1}^{est} = (\mathbf{J}^T \mathbf{J} + \mathbf{C}_M^{-1})^{-1} \mathbf{J}^T \left[(\mathbf{d}^{obs} - \mathbf{d}^{pred}) + \mathbf{J} \mathbf{m}_k^{est} \right],$$

where the superscript *est* indicates estimated (inverted) quantities. \mathbf{J} is the Jacobian matrix that includes the partial derivatives of the data with respect to the model parameters for the k th iteration and \mathbf{C}_M^{-1} is the a priori model covariance matrix that includes the regularization constraints.

In principle, one could simultaneously invert for the P wave velocities, the source functions and the receiver coupling factors, but the strong non-linearity of such an inversion problem makes such an approach unstable. Therefore, we have designed a robust source-function and receiver-coupling estimation scheme that can be applied prior to the Gauss-Newton inversion step in equation (2). Initially, the receiver-coupling factors \mathbf{r} are set to 1.0 and a first estimate of the Green's function G_{ij} is calculated, for example, using a model \mathbf{m}^{ini} based on travelttime inversion of the first breaks. A first estimate of \mathbf{s} is then made using:

$$(3) \quad s_i^{est}(\omega) = \text{mean} \left(\frac{d_{ij}^{obs}(\omega)}{G_{ij}(\omega) \cdot r_j^{ini}(\omega)} \right).$$

Subsequently, s_i^{ini} is set equal to s_i^{est} and first estimates of the receiver-coupling factors are made using:

$$(4) \quad r_j^{est}(\omega) = \text{mean} \left(\frac{d_{ij}^{obs}(\omega)}{G_{ij}(\omega) \cdot s_i^{ini}(\omega)} \right).$$

Values of r_j^{est} are assigned to r_j^{ini} and the procedure is repeated until convergence is achieved (typically after 3 - 5 iterations). The predicted data \mathbf{d}^{pred} computed from equation 1 using \mathbf{m}^{ini} and the "final" estimated source functions and receiver-coupling factors are then the basis for the Gauss-Newton inversion in equation 2. The procedure described above (equations 4 and 5) needs to be repeated prior to every inversion step k (equation 2).

A synthetic example

The experimental configuration for the simulations is shown in Figure 2a. It includes 26 sources and 26 receivers distributed along two boreholes within a medium that contains positive and negative

cross-shaped velocity anomalies. The source is a Ricker wavelet with a central frequency of 1500 Hz. Figure 3a shows the resulting seismic traces for the shot position at 18 m depth. The blue traces represent the simulations using the heterogeneous model in Figure 2, whereas the black traces would be obtained for a homogeneous 2000 m/s model. In Figure 3b, the blue traces are repeated from Figure 2 and red traces are the same as the blue ones except that realistic receiver-coupling factors have been added. The statistics of these factors mimic those of the observed variations in Figure 1. Clearly, the receiver-coupling variations overwhelm the effects of the velocity anomalies (i.e. the differences between the red and blue traces are larger than those between the blue and black traces).

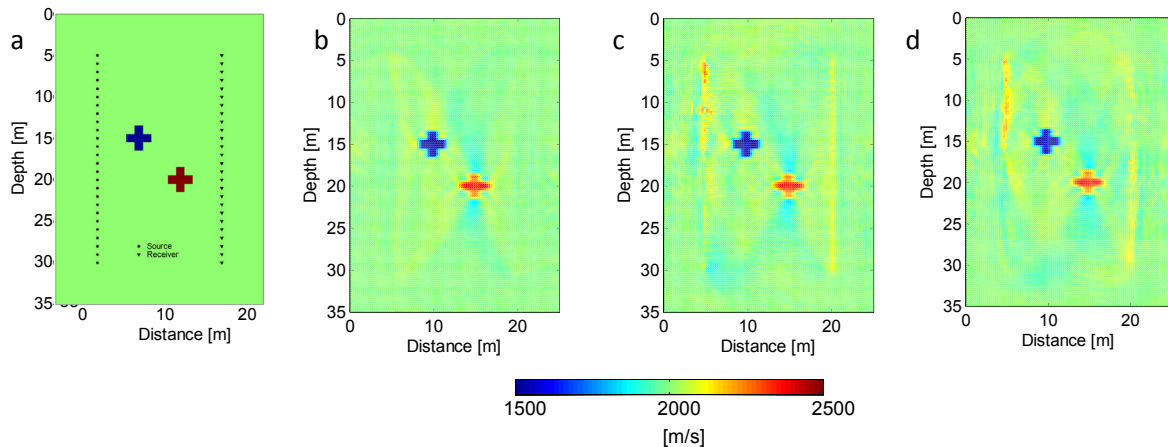


Figure 2: a) Velocity model and source-receiver configuration employed for the synthetic example. b) Tomograms obtained with known source functions and known receiver-coupling factors, c) with unknown source functions and known receiver-coupling factors and c) with unknown source functions and unknown receiver-coupling factors.

Velocity tomograms based on 3 waveform-inversion scenarios are presented in Figure 2b to 2d. For Figure 2b, the known synthetic source function and receiver-coupling factors are employed in equation 1 (i.e. equations 4 and 5 are not required). The two crosses are well resolved in this tomogram. For Figure 2c, the known synthetic receiver-coupling factors are used in equation 1 (i.e. equation 4 is not required), but the "unknown" source function is determined from iterative solutions of equation 3. Although there are minor artifacts along the source and receiver boreholes, the two crosses are again well resolved. Finally, P-wave velocities and "unknown" source functions and "unknown" receiver-coupling factors are determined during the computation of the tomogram in Figure 2d, the quality of which is comparable to that in Figure 2c.

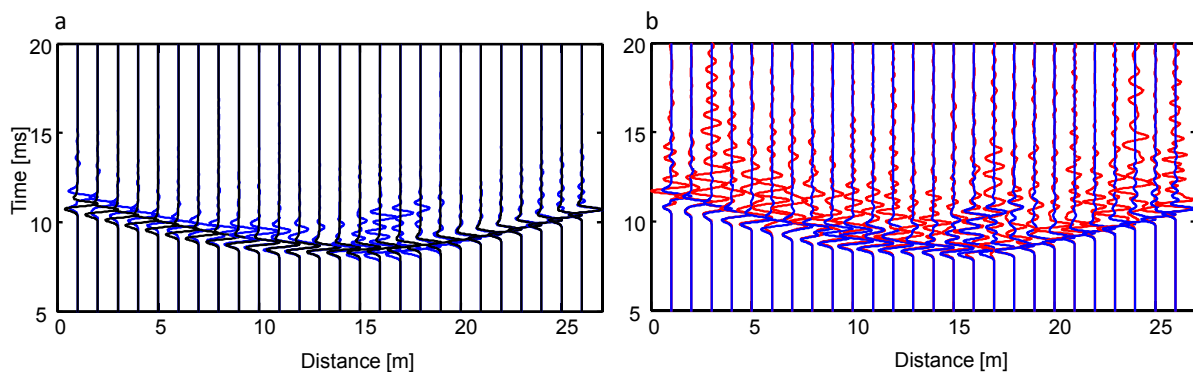


Figure 3: a) Black traces are source gather for the shot position at 18 m depth and a homogeneous velocity model (2000 m/s), whereas the blue traces are a source gather for the same shot position and the heterogeneous model in Figure 2a. b) The blue traces are the same as in a) and the red ones are for the velocity model in Figure 2a with realistic receiver-coupling factors.

Conclusions

A variety of field experiments have indicated that receiver-coupling effects can be very significant, distorting waveform inversions in a major way. Our scheme for estimating unknown source functions and receiver-coupling factors provides a powerful tool for addressing this problem. The scheme has been applied to 2D synthetic acoustic data, but conceptually the methodology can be extended in a relatively straightforward fashion to 2.5D and 3D elastic, visco-elastic and anisotropic media; the scheme for estimating the source function and receiver-coupling factors is only weakly linked to the tomographic inversion algorithm.

Computation of the source functions and receiver-coupling factors using equations 3 and 4 is computationally very efficient, requiring an insignificant amount of computing time compared to that required to calculate the predicted waveforms, the sensitivities and the Gauss-Newton inversion steps. Consequently, such an estimation scheme (or a variant thereof) could be included in every waveform inversion procedure.

Acknowledgments

This work was carried out in the framework of the EC projects ESDRED and ModDeRn. We acknowledge the financial support of the European Commission, NDA, NAGRA and ETH.

References

- Buske, S., Lecomte, I., Nemeth, T., Operto, S. & Sallares, V. [2009] Imaging and inversion --- Introduction. *Geophysics*, **6**(74), WCA1-WCA4.
- Ernst, J. R., Green, A. G., Maurer, H. & Holliger, K. [2007] Application of a new 2D time-domain full-waveform inversion scheme to crosshole radar data. *Geophysics*, **5**(72), J53-J64.
- Manukyan, E., Maurer, H. R., Marelli, S., Greenhalgh, S. A. & Green, A. G. [2008]: Non-intrusive monitoring using seismic tomography at the Mont Terri rock laboratory. In: Annual SEG meeting, Las Vegas, U.S.A.
- Marelli, S., Manukyan, E., Maurer, H. R., Greenhalgh, S. A. & Green, A. G. [2010] Appraisal of waveform repeatability and reliability for crosshole and hole-to-tunnel seismic monitoring of radioactive waste repositories. *Geophysics*, in press.
- Plessix, R.-E. [2008] Introduction: Towards a full waveform inversion. *Geophysical Prospecting*, **6**(56), 761-763.
- Pratt, R. G. [1999] Seismic waveform inversion in the frequency domain, Part 1: Theory and verification in a physical scale model. *Geophysics*, **3**(64), 888-901.
- Pratt, R. G., Shin, C. & Hicks, G. J. [1998] Gauss-Newton and full Newton methods in frequency-space seismic waveform inversion. *Geophysical Journal International*, **2**(133), 341-362.
- Zhou, B. & Greenhalgh, S. A. [2003] Crosshole seismic inversion with normalized full-waveform amplitude data. *Geophysics*, **4**(68), 1320-1330.